Incorporating Loudspeaker Directivity in Array Design for Increased Spatial Aliasing Frequency in Wave Field Synthesis*

Fiete Winter, Frank Schultz, Sascha Spors
Institute of Communications Engineering, University of Rostock, R.-Wagner-Str. 31, 18119 Rostock, Germany,
Email: {fiete.winter; frank.schultz; sascha.spors}@uni-rostock.de

1 Introduction

Wave Field Synthesis (WFS) [1] aims at a physically accurate synthesis of a desired sound field inside a target region. Typically, the region is surrounded by a finite number of discrete loudspeakers. For practical loudspeaker setups, this spatial sampling causes spatial aliasing artefacts and does not allow for an accurate synthesis over the entire audible frequency range. Recently [2], the authors published a geometric model to predict the so-called aliasing frequency up to which the spatial aliasing is negligible for a specific listening position or area. Optimal discretisation schemes to increase this frequency for a given array geometry and desired sound field assuming omnidirectional loudspeakers were presented in [3]. This contribution extends the mentioned prior work by studying the effect of directive actuators on the spatial aliasing properties within the geometric framework. After essential preliminaries have been clarified in Sec. 2, the theory of the geometric model is extended towards directive loudspeakers in Sec. 3. As a concrete example, the aliasing frequency for a piston radiator is derived in Sec. 4. Numerical simulations of the synthesised sound fields are conducted in Sec. 5 to compare the discretisation patterns optimised for omnidirectional and directive loudspeakers. A short conclusion is given, afterwards.

2 Mathematical Preliminaries

A sound pressure field $p(\mathbf{x}, t)$ is a scalar function depending on position $\mathbf{x}$ and time t. Its temporal Fourier transform $P(\mathbf{x}, \omega) = A_P(\mathbf{x}, \omega)\, \mathrm{e}^{+\mathrm{j}\Phi_P(\mathbf{x},\omega)}$ is expressed by its real-valued amplitude $A_P(\mathbf{x}, \omega)$ and phase $\Phi_P(\mathbf{x}, \omega)$, here. The radial frequency $\omega = 2\pi f$ is defined by the temporal frequency f. For an arbitrary sound field fulfilling the linear wave equation, the local wavenumber vector is defined for $\mathrm{e}^{-\mathrm{j}\omega t}$ convention of the Fourier transform as [4, Eq. (15)].

$$\mathbf{k}_P(\mathbf{x}, \omega) := -\nabla\, \Phi_P(\mathbf{x}, \omega) \approx \frac{\omega}{\mathrm{c}}\, \hat{\mathbf{k}}_P(\mathbf{x}, \omega)\,. \tag{1}$$

The speed of sound is denoted as c and is fixed to $343\,\mathrm{m/s}$ for all simulations within this paper. The normalised vector $\hat{\mathbf{k}}_P(\mathbf{x}, \omega)$ describes the local propagation direction of $P(\mathbf{x}, \omega)$ at a given coordinate $\mathbf{x}$. For elementary sound fields such as point and line sources, or plane waves, $\mathbf{k}_P(\mathbf{x}, \omega)$ fulfils the local dispersion relation, i.e. its length is fixed to ω/c. For arbitrary sound fields, this statement is true for asymptotically high frequencies [5, Sec. 5.14].

*This research was supported by grant SP 1295/9-1 of the German Research Foundation (DFG).

As a central concept of the upcoming derivations, the one-dimensional Stationary Phase Approximation (SPA) is used as an integral approximation. Given a complex-valued function $F(u) = A_F(u)\mathrm{e}^{+\mathrm{j}\Phi_F(u)}$ with its phase term rapidly oscillating compared to its slowly changing amplitude, the following approximation of the integral [6, Eq. (3.2)][7, Eq. (2.7.18)]

$$\int_a^b F(u)\mathrm{d}u \approx \sum_{u^*\in[a,b]} F(u^*)\sqrt{\frac{2\pi}{|\Phi_F''(u^*)|}}\mathrm{e}^{+\mathrm{j}\frac{\pi}{4}\mathrm{sgn}(\Phi_F''(u^*))} \tag{2}$$

holds. It constitutes the summation over the stationary points u^* in the interval $[a, b]$, for which the first-order derivative of the phase $\Phi_F'(u^*)$ vanishes and the second-order derivative $\Phi_F''(u^*)$ is non-zero. The integral is approximately zero, if no stationary point is present in $[a, b]$. For a rigorous derivation of the approximation, see [6, Sec. II.3], or [7, Sec. 2.7]. In the context of linear acoustics, the SPA generally becomes more accurate the higher temporal frequency f and the distance between sources and receivers.

3 Geometric Model for WFS with Directive Secondary Sources

WFS is a well-known representative of methods for Sound Field Synthesis (SFS), which pursue an accurate synthesis of a virtual sound field $S(\mathbf{x}, \omega)$ within a defined region Ω, see Fig. 1. In $2^1/_2$-dimensional (2.5D) scenarios [8, Sec. 2.3], Ω is a 2D area. Its boundary $\partial\Omega$ is described as a curve $\mathbf{x}_0 = \mathbf{x}_0(u)$ with $u \in [u_{\min}, u_{\max}]$. The component-wise derivative of $\mathbf{x}_0$ w.r.t. u is denoted as $\mathbf{x}_0'$. It is oriented along the unit tangent vector $\mathbf{t}_0$. The inward pointing boundary normal vector $\mathbf{n}_0$ is perpendicular to $\mathbf{x}_0'$ and $\mathbf{t}_0$. A distribution of loudspeakers is positioned along $\partial\Omega$ as secondary sources (see the loudspeaker symbols in Fig. 1) to synthesise $S(\mathbf{x}, \omega)$. Contrary to own prior investigations [2, 3], the sound field emitted by an individual secondary source is not modelled as an omnidirectional point source, i.e. the free-field 3D Green's function. Instead, the sound radiation is described by a suitable function $G_\mathrm{L}(\mathbf{R}_0\,(\mathbf{x} - \mathbf{x}_0), \omega)$. The rotation matrix $\mathbf{R}_0 = [\mathbf{n}_0, -\mathbf{t}_0]$ ensures that the orientation of the secondary source along $\mathbf{n}_0$ is correctly incorporated. Each loudspeaker is driven by its respective driving function $D(\mathbf{x}_0, \omega)$. The resulting wave field superposition of all secondary sources constitutes the synthesised sound field

$$P(\mathbf{x}, \omega) = \int_{u_{\min}}^{u_{\max}} D(\mathbf{x}_0, \omega)\, G_\mathrm{L}(\mathbf{R}_0\,(\mathbf{x} - \mathbf{x}_0), \omega)\, |\mathbf{x}_0'|\, \mathrm{d}u\,, \tag{3}$$

which is supposed to coincide with $S(\mathbf{x},\omega)$ within Ω.

The generic 2.5D WFS driving function and approximate solution of the integral is given by [2, Eq. (8b)]

$$D(\mathbf{x}_0,\omega) = a_S(\mathbf{x}_0)\sqrt{\mathrm{j}\frac{\omega}{\mathrm{c}}}\sqrt{8\pi d(\mathbf{x}_0)}\,\mathbf{n}_0^{\mathrm{T}}\hat{\mathbf{k}}_S(\mathbf{x}_0,\omega)S(\mathbf{x}_0,\omega)\,. \tag{4}$$

The secondary source selection criterion $a_S(\mathbf{x}_0)$ [4, Eq. (46)] activates only the secondary sources that are oriented along the propagation direction of the virtual sound field. Within this paper, the support $[u_{\min}, u_{\max}]$ already incorporates the selection and all secondary sources described by the curve are assumed to be active. As one systemic artefact in 2.5D synthesis, an inevitable mismatch between the amplitude decay of the synthesised and the virtual sound field occurs. The function $d(\mathbf{x}_0)$ can be used to reference the synthesised sound field to a given contour/location on/at which its amplitude is correct. For more details, see [4].

The practical implementation of WFS implies the discretisation of the continuous Secondary Source Distribution (SSD) as the distance between adjacent loudspeakers cannot be chosen arbitrarily small. For a uniform sampling w.r.t. u the synthesised sound field in (3) is approximated by [3, Eq. (4)]

$$P(\mathbf{x},\omega) \approx P^{\mathrm{S}}(\mathbf{x},\omega) = \sum_{n=0}^{N_0-1} D(\mathbf{x}_0^{(n)},\omega)\,G_{\mathrm{L}}(\mathbf{R}_0^{(n)}(\mathbf{x}-\mathbf{x}_0^{(n)}),\omega)|\mathbf{x}_0'^{(n)}|\Delta_u\,, \tag{5}$$

where the superscript (n) denotes the respective quantity being evaluated at $u = n\,\Delta_u + u_{\min}$. The u-domain sampling distance is defined as $\Delta_u = {}^{u_{\max}-u_{\min}}/_{(N_0-1)}$ with N_0 as the number of secondary sources. It was shown in [2], that the sound field synthesised by the discrete SSD can be separated into its aliasing components

$$P_\eta^{\mathrm{S}}(\mathbf{x},\omega) = \int_{u_{\min}}^{u_{\max}} D(\mathbf{x}_0,\omega)\,G_{\mathrm{L}}(\mathbf{R}_0\,(\mathbf{x}-\mathbf{x}_0),\omega)\,\mathrm{e}^{-\mathrm{j}2\pi\eta\frac{u}{\Delta_u}}\,|\mathbf{x}_0'|\,\mathrm{d}u\,, \tag{6}$$

where η enumerates these components. With the WFS driving function in (4) and amplitude-phase notation of the virtual sound field, the phase term necessary for the SPA of (6) reads

$$\Phi(u) = \Phi_S(\mathbf{x}_0,\omega) + \Phi_{G_{\mathrm{L}}}(\mathbf{R}_0\,(\mathbf{x}-\mathbf{x}_0),\omega) - \frac{2\pi\eta}{\Delta_u}u\,. \tag{7}$$

Using chain and product rule of differentiation allows to formulate the first-order derivative of the phase term as

$$\frac{\partial\Phi(u)}{\partial u} = -\frac{2\pi\eta}{\Delta_u} + \left\langle \nabla\Phi_S(\mathbf{x}_0,\omega)\middle|\mathbf{x}_0'\right\rangle + \left\langle \nabla\Phi_{G_{\mathrm{L}}}(\mathbf{R}_0\,(\mathbf{x}-\mathbf{x}_0),\omega)\middle|\mathbf{R}_0'(\mathbf{x}-\mathbf{x}_0) - \mathbf{R}_0\mathbf{x}_0'\right\rangle\,. \tag{8}$$

The operator $\langle\cdot|\cdot\rangle$ denotes the scalar a.k.a. dot product of two vectors. The element-wise derivative of the rotation matrix w.r.t. u reads $\mathbf{R}_0'$. Setting (8) to zero, solving

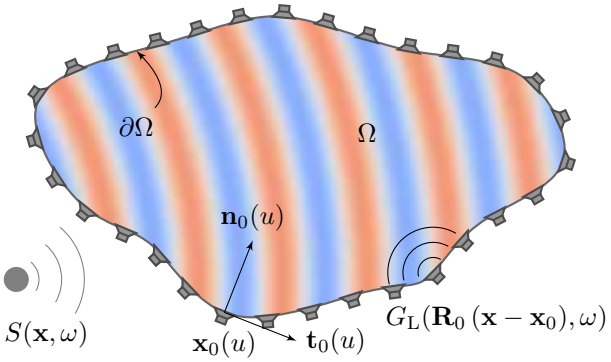

Figure 1: Geometry for Wave Field Synthesis

it for the temporal frequency f, and taking the minimum of $|f|$ over all non-zero η, yields the so-called spatial aliasing frequency $f^{\mathrm{S}}(\mathbf{x}_0,\mathbf{x})$ [2, Eq. (35)]. It defines the frequency, up to which the secondary source at $\mathbf{x}_0$ does not contribute a considerable amount of aliasing to the position $\mathbf{x}$. However, without further assumptions or knowledge about functional relations between f, Φ_S, and $\Phi_{G_{\mathrm{L}}}$ (8) cannot be solved for f. In [2, 3], the propagation direction of the virtual sound field is assumed to be frequency independent, i.e. $\nabla\Phi_S(\mathbf{x}_0,\omega) := -\frac{\omega}{\mathrm{c}}\hat{\mathbf{k}}_S(\mathbf{x}_0)$. For the $\Phi_{G_{\mathrm{L}}}$, the according considerations are presented for the piston model in the upcoming section.

4 Aliasing Frequency for Piston Radiator

A uniformly vibrating membrane is an extensively studied model [9, Secs. 2.11.5/4.6.3/6.7.10] to describe the directive sound radiation of a loudspeaker. Hence, it will be exemplarily considered for $G_{\mathrm{L}}(\mathbf{x},\omega)$. In order to incorporate the piston model into the estimation of the aliasing frequency, the SPA is applied to the underlying integral. Derivations are presented only for one-dimensional membranes along a line as the synthesis scenario is restricted to the horizontal plane. The calculus can however be extended towards surfaces using the multidimensional SPA [7, Sec. 2.7].

The membrane shape is described as a curve $\mathbf{x}_{\mathrm{s}} = \mathbf{x}_{\mathrm{s}}(v)$ depending on the parameter $v \in [v_{\min}, v_{\max}]$ with the according derivative $\mathbf{x}_{\mathrm{s}}'$, tangent $\mathbf{t}_{\mathrm{s}}$, see Fig. 2a. The sound field radiated by the membrane is given by

$$G_{\mathrm{L}}(\mathbf{x},\omega) = \int_{v_{\min}}^{v_{\max}} \frac{\mathrm{e}^{-\mathrm{j}\frac{\omega}{\mathrm{c}}|\mathbf{x}-\mathbf{x}_{\mathrm{s}}(v)|}}{4\pi|\mathbf{x}-\mathbf{x}_{\mathrm{s}}(v)|}|\mathbf{x}_{\mathrm{s}}'(v)|\mathrm{d}v\,. \tag{9}$$

It states a distribution of uniformly driven spherical monopoles along the curve. The integral is solved using the SPA in (2). Setting the first-order derivative of the involved phase term $\Phi(v) = -\frac{\omega}{\mathrm{c}}|\mathbf{x}-\mathbf{x}_{\mathrm{s}}(v)|$ to zero results in

$$\frac{\partial\Phi(v)}{\partial v} = \frac{\omega}{\mathrm{c}}\left\langle \mathbf{x}_{\mathrm{s}}'(v)\middle|\frac{\mathbf{x}-\mathbf{x}_{\mathrm{s}}(v)}{|\mathbf{x}-\mathbf{x}_{\mathrm{s}}(v)|}\right\rangle \overset{!}{=} 0\,. \tag{10}$$

As $\mathbf{x}_{\mathrm{s}}'$ aligns with $\mathbf{t}_{\mathrm{s}}$, the equation requires $(\mathbf{x}-\mathbf{x}_{\mathrm{s}})$ to be perpendicular to the curve. For a given $\mathbf{x}$, the stationary point $\mathbf{x}_{\mathrm{s}}^*(\mathbf{x}) = \mathbf{x}_{\mathrm{s}}(v^*(\mathbf{x}))$ is the orthogonal projection of $\mathbf{x}$ onto the curve. Due to the finite length of the curve, stationary points do only exist for $\mathbf{x}$ inside the grey shaded

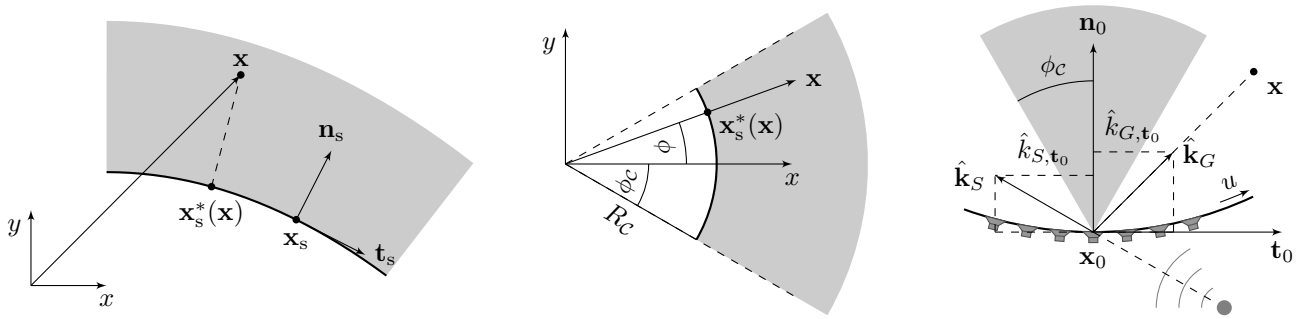

Figure 2: (a) depicts a uniformly driven curved piston (black) line. (b) shows a circular piston of radius $R_\mathcal{C}$ and half-opening angle $\phi_\mathcal{C}$. In (c), the geometry for the spatial aliasing frequency at a single position $\mathbf{x}$ and a virtual point source (grey dot) is depicted: The grey shaded area marks the positions $\mathbf{x}$ for which the sound pressure $G_\mathcal{C}(\mathbf{R}_0\,(\mathbf{x}-\mathbf{x}_0),\omega)$ is non-zero sound.

area depicted in Fig. 2a. For these $\mathbf{x}$, the SPA of (9) is given by

$$G_\mathrm{L}(\mathbf{x},\omega) \approx \sqrt{\frac{2\pi}{\mathrm{j}\frac{\omega}{\mathrm{c}}}} \sqrt{\frac{\rho_\mathrm{s}^*(\mathbf{x})\;|\mathbf{x}-\mathbf{x}_\mathrm{s}^*(\mathbf{x})|}{\rho_\mathrm{s}^*(\mathbf{x})+|\mathbf{x}-\mathbf{x}_\mathrm{s}^*(\mathbf{x})|}}\, \frac{\mathrm{e}^{-\mathrm{j}\frac{\omega}{\mathrm{c}}|\mathbf{x}-\mathbf{x}_\mathrm{s}^*(\mathbf{x})|}}{4\pi|\mathbf{x}-\mathbf{x}_\mathrm{s}^*(\mathbf{x})|}\,, \tag{11}$$

where $\rho_\mathrm{s}^*(\mathbf{x})$ denotes the radius of curvature at $\mathbf{x}_\mathrm{s}(v^*)$. It can be inferred from the phase term $\Phi_{G_\mathrm{L}}(\mathbf{x},\omega) = -\frac{\omega}{\mathrm{c}}|\mathbf{x}-\mathbf{x}_\mathrm{s}^*(\mathbf{x})|$, that the propagation direction of the piston is indeed frequency independent and $\nabla\Phi_{G_\mathrm{L}}(\mathbf{x},\omega) = \frac{\omega}{\mathrm{c}}\hat{\mathbf{k}}_{G_\mathrm{L}}(\mathbf{x})$. Thus, the aliasing frequency can be straightforwardly determined via (8) for arbitrary piston shapes.

As a concrete example for a membrane, a circular arc centred at the origin with a half-opening angle of $\phi_\mathcal{C}$ and a radius of $R_\mathcal{C}$ is chosen, see Fig. 2b. For this case, $|\mathbf{x}-\mathbf{x}_\mathrm{s}^*(\mathbf{x})| = |\mathbf{x}|-R_\mathcal{C}$ and $\rho_\mathrm{s}^*(\mathbf{x}) = R_\mathcal{C}$ and the sound pressure specialises to

$$G_\mathcal{C}(\mathbf{x},\omega) \approx \begin{cases} \sqrt{\frac{2\pi}{\mathrm{j}\frac{\omega}{\mathrm{c}}}}\sqrt{\frac{R_\mathcal{C}}{|\mathbf{x}|}}\;\frac{\mathrm{e}^{-\mathrm{j}\frac{\omega}{\mathrm{c}}(|\mathbf{x}|-R_\mathcal{C})}}{4\pi\sqrt{|\mathbf{x}|-R_\mathcal{C}}} & \text{, if } |\phi| \le \phi_\mathcal{C}\,, \\ 0 & \text{, otherwise.} \end{cases} \tag{12}$$

Thus, the area of non-zero pressure is defined via the half-opening angle $\phi_\mathcal{C}$. For the non-zero case, the phase term and its gradient are given as $\Phi_{G_\mathcal{C}}(\mathbf{x}) = -\frac{\omega}{\mathrm{c}}(|\mathbf{x}| - R_\mathcal{C})$ and $\nabla\Phi_{G_\mathcal{C}}(\mathbf{x}) = -\frac{\omega}{\mathrm{c}}\,\frac{\mathbf{x}}{|\mathbf{x}|}$. Inserting the latter term together with $\nabla\Phi_S(\mathbf{x}_0,\omega) = -\frac{\omega}{\mathrm{c}}\hat{\mathbf{k}}_S(\mathbf{x}_0)$ into (8), allows to formulate the aliasing frequency as [2, Eqs. (35)]

$$f^\mathrm{S}(\mathbf{x}_0,\mathbf{x}) = \frac{\mathrm{c}}{\Delta_u|\mathbf{x}_0'(u)||\hat{k}_{S,\mathbf{t}_0}(\mathbf{x}_0) - \hat{k}_{G,\mathbf{t}_0}(\mathbf{x}-\mathbf{x}_0)|}\,, \tag{13}$$

The explanatory geometry is shown in Fig. 2c: $\hat{k}_{S,\mathbf{t}_0}(\mathbf{x}_0)$ denotes the tangential component of the normalised wavenumber vector $\hat{\mathbf{k}}_S$ for the virtual sound field. It is equal to the cosine of the angle between the tangent $\mathbf{t}_0$ and the propagation direction of the virtual sound field at $\mathbf{x}_0$. $\hat{k}_{G,\mathbf{t}_0}(\mathbf{x}-\mathbf{x}_0)$ denotes the tangential component of the normalised wavenumber vector $\hat{\mathbf{k}}_G$ of the Green's function. It is equal to the cosine of the angle between $\mathbf{t}_0$ and $\mathbf{x}-\mathbf{x}_0$.

The formula for the aliasing frequency in (13) is the same as for the omnidirectional case [2, Eq. (35)], but it has to be further taken into account, that the secondary source only contributes aliasing to $\mathbf{x}$, if its directivity is non-zero, see grey-shaded area in Fig. 2c. This finally leads to

$$f_\mathcal{C}^\mathrm{S}(\mathbf{x}_0,\mathbf{x}) = \begin{cases} f^\mathrm{S}(\mathbf{x}_0,\mathbf{x}) & \text{, if } G_\mathcal{C}(\mathbf{R}_0\,(\mathbf{x}-\mathbf{x}_0),\omega) \neq 0 \\ \infty & \text{, otherwise,} \end{cases} \tag{14}$$

as the aliasing frequency incorporating the restricted radiation range of the circular arc piston. Since $f_\mathcal{C}^\mathrm{S}(\mathbf{x}_0,\mathbf{x}) \geq f^\mathrm{S}(\mathbf{x}_0,\mathbf{x})$, it is obvious, that the additional directivity potentially leads to a stronger suppression of aliasing. One may further define [2, Eq. (38)]

$$f_\mathcal{C}^\mathrm{S}(\mathbf{x}_0) = \min_{\mathbf{x}\in\Omega_\mathrm{l}} f_\mathcal{C}^\mathrm{S}(\mathbf{x}_0,\mathbf{x}) \tag{15}$$

as the aliasing frequency for an extended region Ω_l instead of the single position $\mathbf{x}$. In [3, Sec. 4.2], a method to maximise the overall aliasing frequency, i.e. the minimum of $f_\mathcal{C}^\mathrm{S}(\mathbf{x}_0)$ over all active secondary sources, by adjusting the spatial sampling of the SSD for a given N_0. For this, the equation [3, Eqs. (14)/(15)]

$$n\int_{u_\mathrm{min}}^{u_\mathrm{max}} \frac{1}{f_\mathcal{C}^\mathrm{S}(\mathbf{x}_0(\mu))}\mathrm{d}\mu = (N_0-1)\int_{u_\mathrm{min}}^{u_\mathrm{opt}(n)} \frac{1}{f_\mathcal{C}^\mathrm{S}(\mathbf{x}_0(\mu))}\mathrm{d}\mu \tag{16}$$

is solved for $u_\mathrm{opt}(n)$ by combining numerical integration and root finding algorithms. The resulting optimised positions are given by $\mathbf{x}_0(u_\mathrm{opt}(n))$.

5 Simulations

The derived aliasing frequency for the circular arc position will be compared to the omnidirectional case using exemplary numerical simulations of the synthesised sound fields. Furthermore, the effect of differently optimised SSD spacings is shown. A virtual point source at $\mathbf{x}_\mathrm{ps} = [0, 2.5, 0]^\mathrm{T}\,\mathrm{m}$ is synthesised by a linear SSD of 3 m length, see black dots in Fig. 3. For the circular arc piston, an half opening angle of 30° is chosen. The region of interest Ω_l, for which the aliasing frequencies are optimised, is defined as a circular area (red). As shown in Fig. 3a and 3b, the directivity leads to an improvement of the spatial aliasing even for the uniform discretisation pattern. However, strong artefacts inside the red circle are observable in the synthesised sound field for

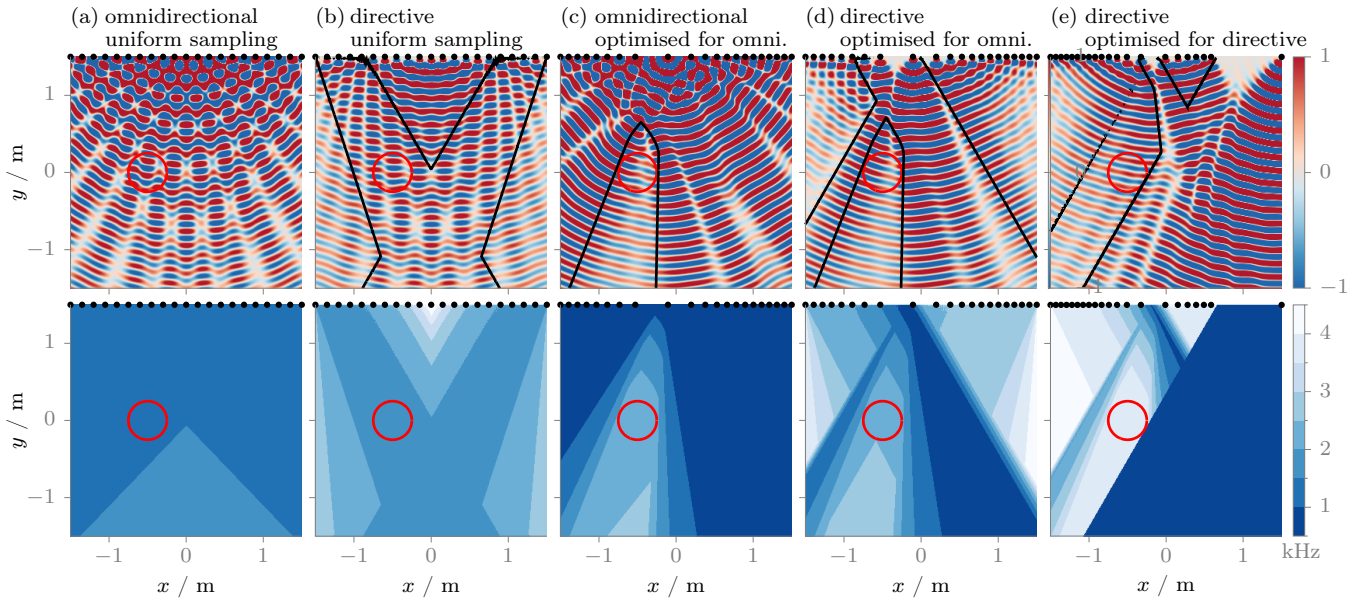

Figure 3: The plots in the top row illustrate a monochromatic ($f = 2\,\mathrm{kHz}$) virtual point source at $\mathbf{x}_{\mathrm{ps}} = [0, 2.5, 0]^{\mathrm{T}}\,\mathrm{m}$ synthesised by a linear SSD ($N_0 = 21$, black dots) with different spacing patterns. The directivity of the secondary source and sampling optimisation strategy are given in title. The circular area Ω_{l} located at $[-0.5, 0, 0]^{\mathrm{T}}\,\mathrm{m}$ with a radius of 0.25 m is indicated by the red circle. The black line indicate position where the aliasing frequency is equal to 2 kHz. This frequency is shown in the bottom plots in more detail. A discrete colormap is used for better visibility.

both secondary source types. Fig. 3c and 3d show the results for the SSD spacing optimised w.r.t. the omnidirectional aliasing frequency defined by (13): The SSD is less densely sampled in middle of the distribution. Compared to the respective aliasing frequency for the uniform case, an increase about a factor of ≈ 1.5 inside Ω_{l} is achieved. The spacing is further optimised for the directive case using (14) as the criterion. It can be observed in Fig. 3e, that a large gap in the SSD is present on its right-hand side. This is reasonable as the opening angle of circular arc piston is small enough, that secondary sources in this part do not affect Ω_{l}. Thus, the gap allows to the increase increase the density of the more relevant left-hand side of the array. Compared to the uniform sampling, an increase of the aliasing frequency about the factor of ≈ 2.2 is achieved.

6 Conclusion

This paper investigated on the connection between the directivity of the secondary sources involved in WFS and spatial aliasing artefacts occurring in the synthesised sound field. A geometric model to predict spatial aliasing was extended towards directive actuators allowing for a more accurate prediction of the aliasing frequency. The numerical simulations confirm, that optimised SSD design can be further improved by considering the directional properties of the deployed loudspeakers. As the involved approximations of the piston radiator model led to rather simplistic radiation properties, future work has to incorporate the effect of more complex and frequency-dependent directivity patterns. Moreover, the combination of SSD spacing and array curvature has to be discussed within the geometric framework.

References

[1] A. J. Berkhout. "A Holographic Approach to Acoustic Control". In: *J. Aud. Eng. Soc.* 36.12 (1988), pp. 977–995.

[2] F. Winter, F. Schultz, G. Firtha, and S. Spors. "A Geometric Model for Prediction of Spatial Aliasing in 2.5D Sound Field Synthesis". In: *IEEE/ACM Transactions on Audio, Speech, and Language Processing* (2019).

[3] F. Winter, F. Schultz, and S. Spors. "Array Design for Increased Spatial Aliasing Frequency in Wave Field Synthesis Based on a Geometric Model". In: *Proc. of German Annual Conference on Acoustics (DAGA)*. Rostock, Germany, Mar. 2019, pp. 463–466.

[4] G. Firtha, P. Fiala, F. Schultz, and S. Spors. "Improved Referencing Schemes for 2.5D Wave Field Synthesis Driving Functions". In: *IEEE/ACM Transactions on Audio, Speech, and Language Processing* 25.5 (2017), pp. 1117–1127.

[5] L. E. Kinsler, A. R. Frey, A. B. Coppens, and J. V. Sanders. *Fundamentals of Acoustics*. 4th Ed. John Wiley & Sons, Inc., 1999.

[6] R. Wong. *Asymptotic Approximations of Integrals*. Vol. 34. Classics in Applied Mathematics. Philadelphia, PA: Society for Industrial and Applied Mathematics (SIAM), 2001.

[7] N. Bleistein. *Mathematical Methods for Wave Phenomena*. Orlando, USA: Academic Press, 1984.

[8] E. N. G. Verheijen. "Sound Reproduction by Wave Field Synthesis". PhD thesis. Delft University of Technology, 1997.

[9] E. G. Williams. *Fourier Acoustics: Sound Radiation and Nearfield Acoustical Holography*. Academic Press, 1999.